Search for deeply bound pionic states in ^{208}Pb via radiative atomic capture of negative pions

K. J. Raywood, J. B. Lange, G. Jones,* and M. Pavan†
Department of Physics, University of British Columbia, Vancouver, British Columbia, Canada V6T 1Z1

M. E. Sevior
School of Physics, University of Melbourne, Parkville Victoria, 3052, Australia

D. A. Hutcheon,‡ A. Olin,§ D. Ottewell, and S. Yen
TRIUMF, 4004 Wesbrook Mall, Vancouver, British Columbia, Canada V6T 2A3

S. J. Lee and K. S. Sim
Department of Physics, Korea University, Seoul 136-701, Korea

A. Altman
Direx Medical Services, P.O. Box 4190, Petah-Tikva, 41920 Israel

E. Friedman
Racah Institute of Physics, Hebrew University, Jerusalem 91904, Israel

A. Trudel
Simon Fraser University, Burnaby, British Columbia, Canada V5A 1S6
(Received 23 September 1996)

A search for narrow, deeply bound pionic atom states via atomic radiative capture of negative pions in a target of ^{208}Pb was carried out for pion kinetic energies of 20 and 25 MeV. Although no clear signature of any such gamma ray emission could be observed in the data, fits of the gamma ray spectra between the energies of 12 and 42 MeV involving a quadratic background together with a pair of peaks ($1s$, $2p$) whose relative intensity was taken from theory yielded an overall strength for the peaks which are consistent (to a 67% confidence level) with radiative capture whose integrated cross section is 20.0 ± 10.0 μb/sr at 90° for 20 MeV incident pions. A lower probability (40% confidence level) result was obtained when the fit was carried out without the peaks included, just the continuum background. [S0556-2813(97)04205-2]

PACS number(s): 25.80.Ls, 27.80.+w, 36.10.Gv

I. INTRODUCTION

Narrow widths for deeply bound states in pionic atoms have been predicted on the basis of pion-nucleus optical potentials that provide a good fit to the available data on strong interaction effects in pionic atoms [1,2]. These potentials contain a repulsive s-wave term and an attractive p-wave term. The existing pionic atom data consist essentially of the measured energies of x rays emitted during deexcitation of the pionic atoms produced when negative pions are stopped in a target. Nuclear absorption, however, terminates the atomic cascade, preventing the population of even more deeply bound pionic atom states, once the levels involved have strong interaction widths larger than the radiation widths.

The p-wave term of the pion-nucleus potential contributes most of its effect in the surface region of the nucleus and is known to be closely related to the free πN interaction. In contrast, the s-wave component, whose importance increases with increasing binding energy, is effective throughout the nuclear volume and therefore holds promise for providing information on medium modification of the interaction. The termination of the observable transitions, however, prevents this term from yielding its full effect. In fact, after years of analysis of pionic atoms [3,4], open problems concerning ''missing'' s-wave repulsion still exist [4]. It is therefore of great interest to study pionic atom states whose binding energies are greater than those previously studied in order to elucidate the strong interaction effects related to the s-wave term in the pion-nuclear potential.

In ^{208}Pb$*\pi^-$, for example, the last experimentally observable x-ray line is $4f \rightarrow 3d$ [4,5]. The resulting $3d$ binding energy is 2863 ± 2 keV and its width is 47 ± 4 keV. *Calculated* values of the binding energies (widths) of the $2p$ and $1s$ states are 5100 (300) keV and 6760 keV (450) keV, respectively [4]. These are sufficiently narrow that the states should be well separated.

The possibility of direct production of pions into these deeply bound levels has been proposed as a means of studying them [2,6–10]. None of the experiments which immediately followed these suggestions, however, achieved a positive result [11–13]. Recently, however, a group using the

*Electronic address: garth@triumf.ca
†Current address: MIT, Cambridge, Massachusetts.
‡Electronic address: hutcheon@alph04.triumf.ca
§Electronic address: olin@triumf.ca

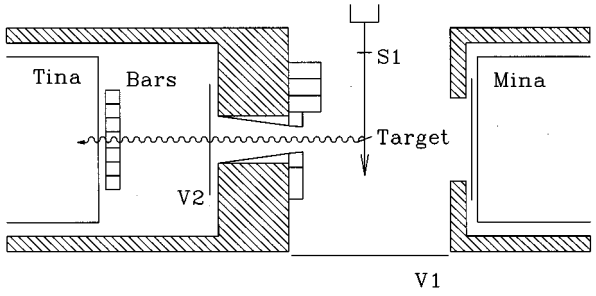

FIG. 1. Experimental configuration for the 1994 experiment.

Fragment Separator facility (FRS) at GSI has reported [14] the detection of a bound $2p$ atomic state in ^{207}Pb via the reaction $^{208}\mathrm{Pb}(d,{}^3\mathrm{He})^{207}\mathrm{Pb}*\pi^-$. These results yield a width for the $2p$ state, Γ_{2p}, of <0.7 MeV and a binding energy equal to that predicted, 5.16 MeV.

Nieves and Oset [15], on the other hand, considered the possibility of producing such atoms by the radiative capture of low-energy pions. They concluded that the (π^-,γ) atomic capture reaction on ^{208}Pb was a particularly favorable choice. The signature, in this case, is a photon whose energy is the sum of the kinetic energy of the beam pion and the binding energy of the atomic state. In order to avoid background gammas from nuclear deexcitation and π^0 decay, an incident pion energy of $\sim$20 MeV was recommended [15]. These theoretical results have recently been confirmed (to within 35%) by Morimatsu and Yazaki [16] who carried out their calculations for the case of 10 MeV incident pions using a Green's function approach.

A measurement of this kind, however, involves a number of challenging experimental problems. The very small cross section expected ($\sim$10 μb/sr) requires the use of intense pion beams together with a gamma ray detector having both large solid angle and high efficiency for detecting the gamma rays. Thus, the ideal detector should possess (a) high efficiency, because of the low cross section involved, (b) an energy resolution of better than a few hundred keV when detecting photons of 20–30 MeV, (c) good discrimination against neutrons because of the intense background arising from (π^-,n) reactions in the target, and (d) negligible production of low-energy tails arising from detection of γ rays of 50–150 MeV. By employing a large, segmented NaI detector system together with an appropriate array of veto counters and extensive shielding, we were able to achieve a sensitivity to (π^-,γ) cross sections which, when integrated over a bin width of several MeV, approached the level predicted by Nieves and Oset [15], viz., $\sim$10 μb/sr.

II. EXPERIMENTAL CONFIGURATION

The experiment was carried out on the low-energy pion channel M13 at TRIUMF [17,18]. Figure 1 shows the arrangement of detectors and shielding used in the target region. The plastic scintillator $S1$, 3.2 cm $\times$ 3.2 cm and 0.16 cm thick, was mounted 31.5 cm upstream of the Pb target. Measurement of particle flight times down the beam channel to $S1$ enabled the pions in the beam to be cleanly distinguished from contaminant electrons and muons. A large, thin plastic scintillator ($V1$) vetoed those accidental triggers associated with pions traversing the Pb target without suffering absorption. It also vetoed those events corresponding to a pion which decayed to a muon after passing through $S1$. The photon detector, shielded by steel and lead together with collimators to ensure that the photons came from the target, consisted of a relatively thin (5.1 cm) NaI converter segmented into ''bars'' [19] backed by a large-volume NaI crystal (''TINA'') [20], with the two systems operated in coincidence. For an energy deposition requirement of 7 MeV in the bars and 2 MeV in TINA, the efficiency of this system for detecting 25 MeV photons was estimated, using the EGS4 shower code [21], to be about 35% of that of a single, large, monolithic NaI crystal, while the response to neutrons was an order of magnitude smaller than that of the single crystal. With even a modest flight path, the timing resolution of the converter (1.7 ns) was adequate for distinguishing photons from the fast neutrons emitted by the Pb target. The photon detector subtended a total solid angle at the target of 85 msr.

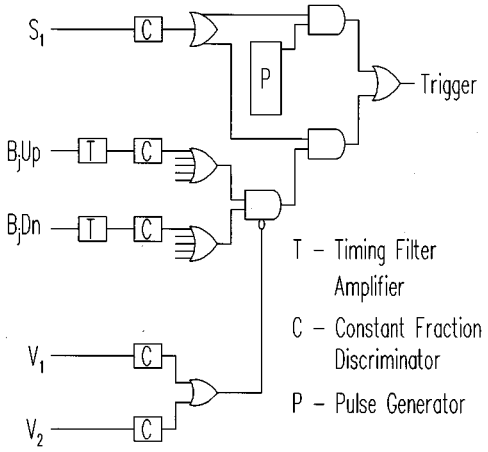

FIG. 2. The master trigger circuit.

The use of a large-volume backup detector in this way served to reduce the low-energy tail from $\approx$100 MeV photons to a manageable level. The requirement of energy deposition in both detectors also served to discriminate against fast neutrons. The principal limitation of such a detector system, however, was its limited energy resolution ($\sim$3 MeV at 25 MeV).

A 6.0-mm-thick veto scintillator ($V2$) vetoed the signals produced in the NaI counters by charged particles emitted by the target. An additional NaI monitor counter MINA [20], located at 90° to the target, but on the opposite side of the beam line to the primary photon detection system, was used to monitor π^0 decays during the experiment.

Not shown in Fig. 1 is a set of nine narrow, thin plastic scintillators (the ''hodoscope'') located at a momentum-dispersed intermediate focus of M13. These hodoscope signals enabled determination of the momentum of individual pions to within 1% while allowing the full 7% momentum acceptance of M13 to be utilized.

The circuit diagram used in the experiment is illustrated in Fig. 2. Scintillator pulse-height and timing information were digitized by Camac analog-to-digital converters (ADC's) (LRS 2249A) and time-to-digital converters (TDC's) (LRS 2228A) with the data recorded on an event-by-event basis on magnetic tape for off-line analysis. Timing

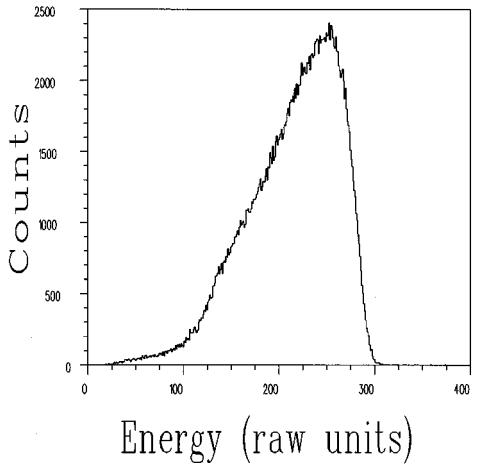

FIG. 3. Typical energy loss spectrum in a converter bar counter for 25 MeV electrons.

of the NaI signals was accomplished using timing filter amplifiers (Ortec 474) in conjunction with constant-fraction discriminators (Tennelec TC455). The data acquisition system was triggered by two types of events: (1) an electronic coincidence ($S1 \cdot V1 \cdot Up \cdot Dn \cdot V2$), where Up and Dn refer to the signals from each end of the converter bars, and (2) ($S1 \cdot P$), where P was the output of a pulse generator. The (2) events thus constituted a sampled fraction (typically $\sim$40%) of the pion beam hitting the in-beam counter $S1$.

The target, consisting of lead enriched in ^{208}Pb, was in the form of metal foils of 408 mg/cm^2 total thickness, supported by fine thread to minimize the mass of nontarget material intercepting the beam. The fraction of the pion beam detected by counter $S1$ which also passed through the target material was measured by replacing the target with an ''antitarget'' — a mask which stopped all pions except those passing through a hole cut to the same size as the target. The ratio of the resulting ($S1 \cdot V1$) coincidence rate to the $S1$ rate thus represented the fraction of pions hitting the Pb target.

III. EXPERIMENTAL SETUP

A. Photon response

The first stage of the experiment consisted of determining the pulse-height responses of the NaI detectors to photons of 20–30 MeV. This calibration was actually carried out by measuring the detector response to electrons, since the response of a NaI detector to energetic electrons is very similar to its response to photons of the same energy. Small differences due to different energy losses in dead layers were estimated by simulations based on the EGS4 shower code. For this electron response, the experimental target was removed and the NaI detector positioned at 0° to the incident beam. The M13 channel was tuned to a momentum of 25 MeV/c and the electron component of the beam selected by a timing cut. For electrons of this energy, small enough that most of the electron-gamma shower was contained in the converter, a spectrum like that of Fig. 3 was obtained. These measurements were repeated at momenta of 50 and 75 MeV/c in order to confirm the linear relationship between the midpoint of the leading edges of these distributions and the electron beam energy.

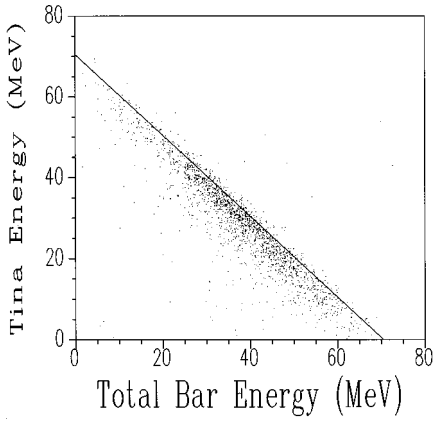

FIG. 4. A calibration scatter plot of energy deposited in TINA versus the energy deposited in the bars for 75 MeV incident electrons.

Using 75 MeV electrons, the TINA crystal was then calibrated in terms of the known converter calibration. Since the electromagnetic shower which emerges from the converter when detecting an energetic electron deposits its remaining energy in TINA, the TINA calibration was carried out by analyzing scatter plots of the total energy deposited in the converter versus the ADC signal from each of the NaI phototubes. A typical scatter plot (for TINA phototube number three) is shown in Fig. 4. Normalization of the individual TINA phototube signals was carried out by fitting straight lines to the upper edges of the data for each scatter plot of this type, as demonstrated in Fig. 4. Normalization was achieved when the straight lines had slopes of -1, indicative of the intercepts of the lines with both the abscissas and ordinates equaling the incident electron beam energy. Figure 5 is a representative spectrum from the photon detector (TINA+converter) obtained using $\sim$75 MeV electrons. Assuming, as discussed earlier, that the interaction of $\sim$75 MeV gamma rays is similar to that of electrons, the resulting gamma ray resolution was $\sim$10%, viz., 7.0 MeV, full width

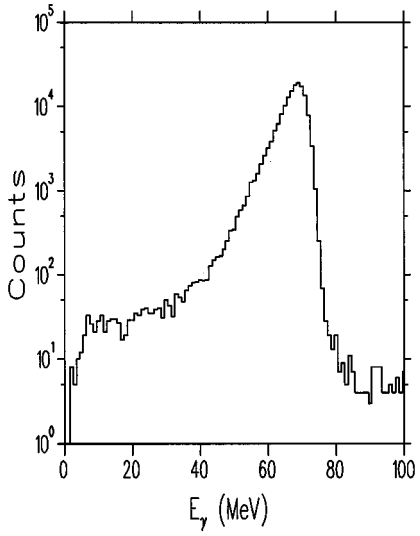

FIG. 5. An energy spectrum in the NaI detector array produced by a monenergetic beam of 75 MeV electrons.

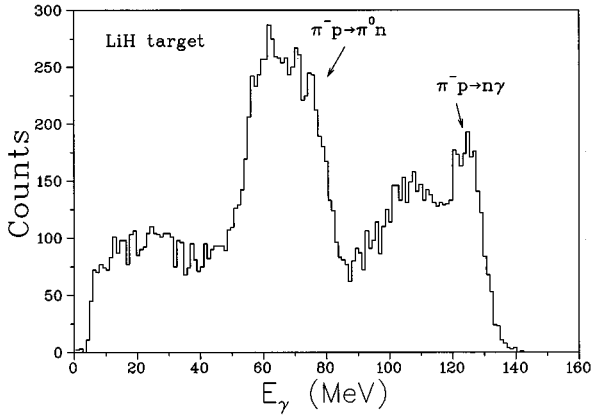

FIG. 6. Photon energy spectrum produced for π^- stopped in a LiH target.

at half maximum (FWHM). A similar spectrum obtained for 25 MeV electrons yielded a resolution of 3.0 MeV, FWHM.

B. Background discrimination

Background signals due to charged particles emanating from the target were readily rejected using the plastic veto scintillator ($V2$).

Neutron backgrounds were a greater problem, however. Our principal method for discriminating against them was based on particle flight times between the in-beam scintillator ($S1$) and the converter. In order to optimize the gamma-neutron timing difference, it was necessary to correct for the dependence of the converter timing on pulse amplitude. For this, the NaI detector was positioned at 90° to the beam, and a LiH target thick enough to stop the 20 MeV pions was placed at the target location. The use of LiH optimized the number of pions absorbed on free protons (for LiH the fraction of the pions captured by the protons is 3.5% [22], a fraction more than twice as large as that for other common hydrogenous materials like CH_2). A typical total energy spectrum taken using the LiH target during the 1993 run is shown in Fig. 6. Clearly visible are both the pion radiative capture peak ($\pi^- p \to n\gamma$) and the photons corresponding to the π^0 ''box'' arising from pion charge exchange. These photons are Doppler shifted into a ''box'' spectrum because of the motion of the π^0.

A typical (raw) time distribution obtained using the LiH target is shown in Fig. 7(b). Figure 7(a), a scatter plot of pulse height in the converter against this time-of-flight signal, indicates the extent to which the time measurement depended on pulse height, a dependence which was significant in the energy region of interest: 20–30 MeV. By fitting the short flight-time region (principally due to gamma rays) with a suitable phenomenological function, the timing spectrum could be corrected for this pulse-height dependence. The resulting spectra, shown in Figs. 7(c) and 7(d), demonstrate the effectiveness of this technique.

In order to further suppress the neutron background, a threshold discrimination level of 7 MeV was applied to the aggregate energy spectra of the converter, and 2 MeV to the TINA signal. These constraints reduced the neutron contribution in the region of interest by more than 50%, while the gamma portion of the spectrum was much less affected (Fig. 8).

IV. EXPERIMENT

The atomic radiative capture measurements were carried out using the ^{208}Pb target with the gamma detector posi-

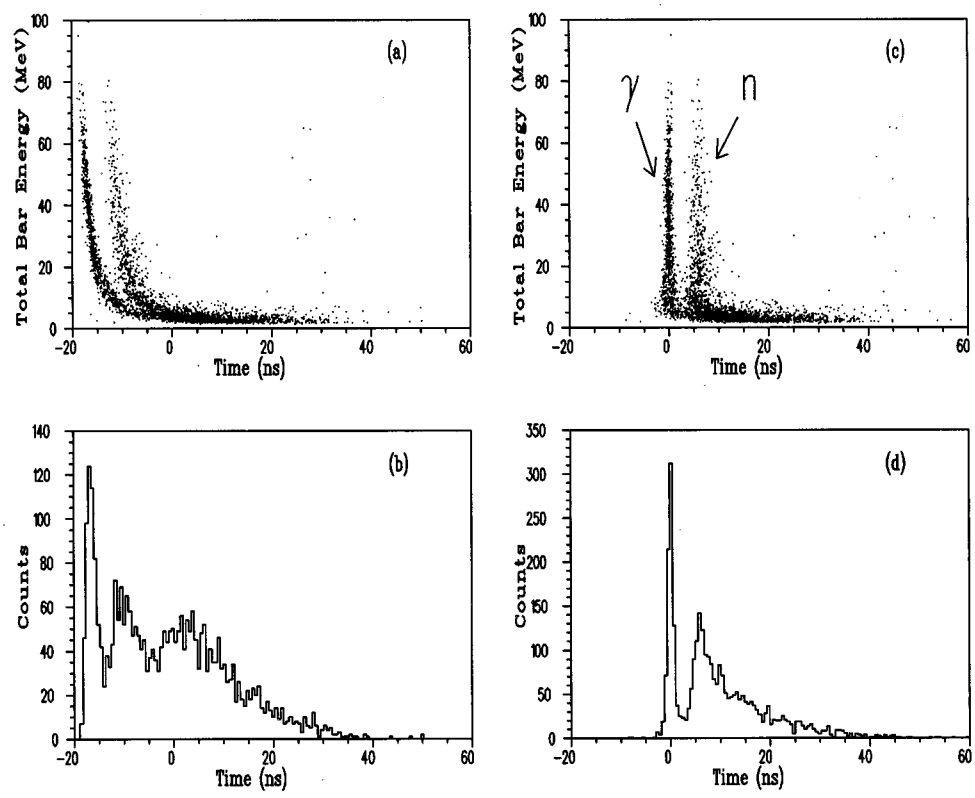

FIG. 7. The raw (a) and corrected (c) two-dimensional scatter plots of energy vs time-of-flight spectra from $S1$ to the converter. The projected one-dimensional time-of-flight spectra are provided in (b) and (d), respectively.

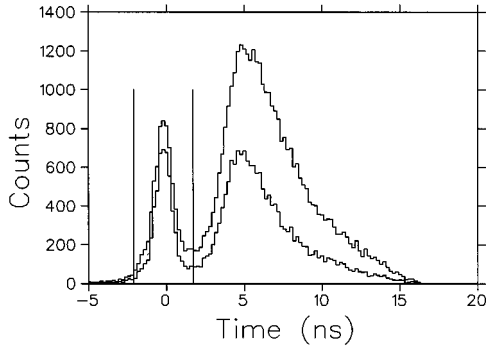

FIG. 8. Timing spectra for 25 MeV π^- on ^{208}Pb both before and after threshold discrimination was applied to the NaI detectors. While the neutron peak was reduced by 53%, the gamma peak was only reduced by 29%. The timing window used to select the gamma rays is also indicated.

tioned at 90° to the beam. Two pion beam energies were used, 20 MeV, the energy at which a theoretical value for the cross section was available [15], and 25 MeV, an energy that was chosen partly as an experimental check, since a change in beam energy should result in an equal change in the energy of the radiated photons. At each energy the runs with target in place were interspersed with no-target runs. The data were collected in two distinct blocks of beam time, one in 1993 and one in 1994. The first of these was intended primarily as a ''proof of concept'' measurement and so was characterized by rather limited statistics. The following year, the experiment was repeated with slight modifications in order to provide both better statistics and better background suppression. The details of these two running periods are summarized in Table I. Although the ''hodoscope'' was employed in the pion channel during the 1993 run, an instrumental fault precluded its use during the 1994 runs.

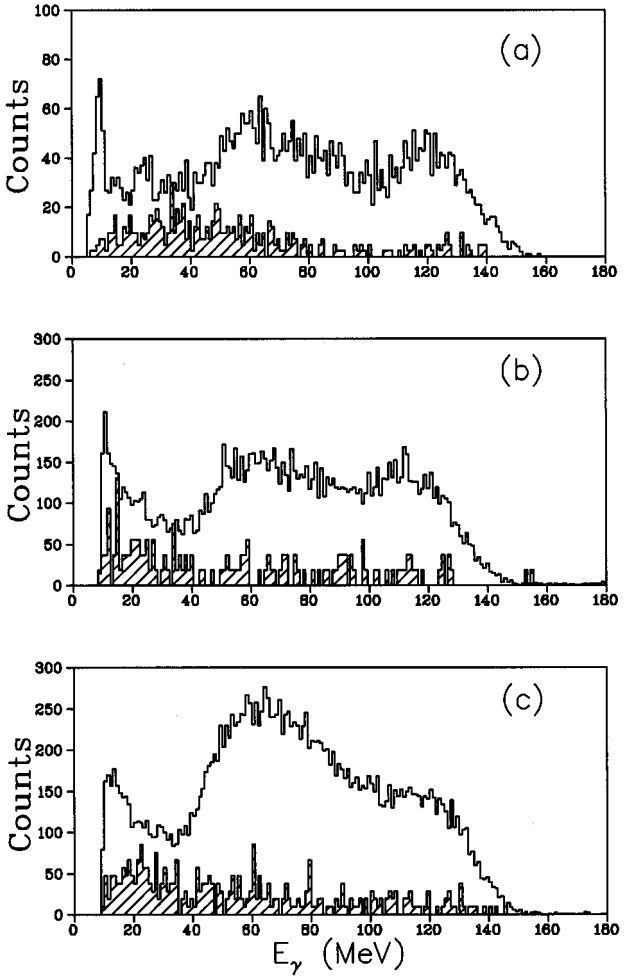

FIG. 9. Gamma energy spectra for ^{208}Pb$(\pi^-,\gamma)X$. (a) $T_\pi = 20$ MeV (1993). (b) $T_\pi = 20$ MeV (1994). (c) $T_\pi = 25$ MeV (1994). The shaded area is the no-target background.

V. RESULTS

The total energy spectra characterizing the three data sets obtained using the ^{208}Pb target are shown in Fig. 9. Radiative transitions to the deeply bound π^- atomic states would be expected to yield peaks at about 25 MeV for the 20 MeV incident pions, and at about 30 MeV for the 25 MeV pions.

Of potential concern was the possible contribution, in the energy range of interest (20–40 MeV), of the low-energy ''tails'' characterizing the response of the gamma detector to higher energy photons. Figure 5, however, shows that the magnitude of these tails for our apparatus was very small (15 counts/MeV for an integrated count of 10 000 in the peak). For the spectra of Fig. 9, this contribution, when integrated over all the higher-energy gamma rays (π^0 box, as well as the nucleonic radiative capture), corresponds to about 1/4 of the observed signal (that exceeding the no-target background).

Another indication of the amount of photon ''leakage'' from the π^0 box into the energy region of interest in the final spectra was provided by the NaI monitor counters. Since neutral pions decay into a pair of gamma rays, the coincident detection of signals from this monitor counter together with

TABLE I. Experimental configuration specifications.

	1993 runs	1994 runs
Target-to-bars distance	56 cm	88 cm
Momentum spread of beam	7%	3%
Hodoscope	In use	Not used
Target dimensions	5.5 cm× 5.0 cm× 0.036 cm	5.5 cm× 5.0 cm× 0.036 cm
*V*1 dimensions	56 cm (vert) × 43 cm (horiz)	51 cm (vert) × 55 cm (horiz)
Pions on target	50%	67% (20 MeV), 82% (25 MeV)
NaI monitor counter	2×2 array, 8400 cm^3	single counter, 36 600 cm^3

TABLE II. Experimental characteristics of the three data runs.

	20 MeV (1993)	20 MeV (1994)	25 MeV (1994)
T (cm^{-2})	1.31×10^{21}	1.31×10^{21}	1.31×10^{21}
$\Delta\Omega$ (msr)	90	85	85
N_{inc}	2.78×10^{10}	8.10×10^{10}	11.28×10^{10}
λ	0.94	0.91	0.98
η	0.32	0.32	0.36
EB1's (MeV)	6.0	5.0	6.5
G (μb/sr)	1.0	0.38	0.23

the normal photon detector flags their production, and hence identifies those ''low-energy'' photons arising from this process. It was found that ~10% of the events of this kind, where the energy deposited in the monitor counter was appropriate to that of the π^0 box, were associated with an energy deposition in the primary photon detector in the 10–40 MeV range. This corresponds to ~ twice that expected from the direct estimate of the tail contribution of photons from π^0 decay in the photon detector (however, because of the very limited statistics associated with these coincident counts, this deviation is only 2σ). This contribution to the continuum background occurs predominantly in the upper region of the 10–40 MeV range, however, as the Doppler effect associated with the motion of a π^0 produced by charge exchange with a nuclear target causes the tail of the π^0 box to extend somewhat below 40 MeV. Thus, a monotonically increasing spectral shape in the 10–40 MeV range is the expected contribution of such tails. The monotonic *decrease* with increasing energy observed in the lower part of the 10–40 MeV range of the photon spectrum is probably attributable to a pileup of lower-energy nuclear deexcitation gamma rays.

An interesting feature of Fig. 9 is the rapid increase (from ~1.15 to 1.75) in the ratio of the charge exchange to the direct nuclear radiative capture cross section for ^{208}Pb as the incident pion energy increases from 20 to 25 MeV.

Another point of interest is the relative size, for 20 MeV pions, of the direct nuclear capture cross section leading to high-energy photons (~100 MeV) relative to the total absorption cross section. Using the calculated detection efficiency of ~75% for the NaI counter system, and the G factors of Table II, the average cross section for the two 20 MeV runs (1993 and 1994) is about 1300 μb/sr at 90° (assuming that the ''peak'' at ~100 MeV can be approximated as Gaussian in shape). Assuming isotropy, a total cross section of ~16 mb results, compared to the total absorption cross section of ~2000 mb [23]. This ratio of cross sections (0.8%) is only slightly less than the few percent probability characterizing the production of high-energy radiative capture gamma rays through the capture of *stopped* π^- [24].

VI. ANALYSIS

The double differential cross section is given by

$$\frac{d^2\sigma}{d\Omega dE}=\frac{n}{T\Delta\Omega\Delta E N_{\rm inc}\lambda\eta}=G\frac{n}{\Delta E}, \qquad (1)$$

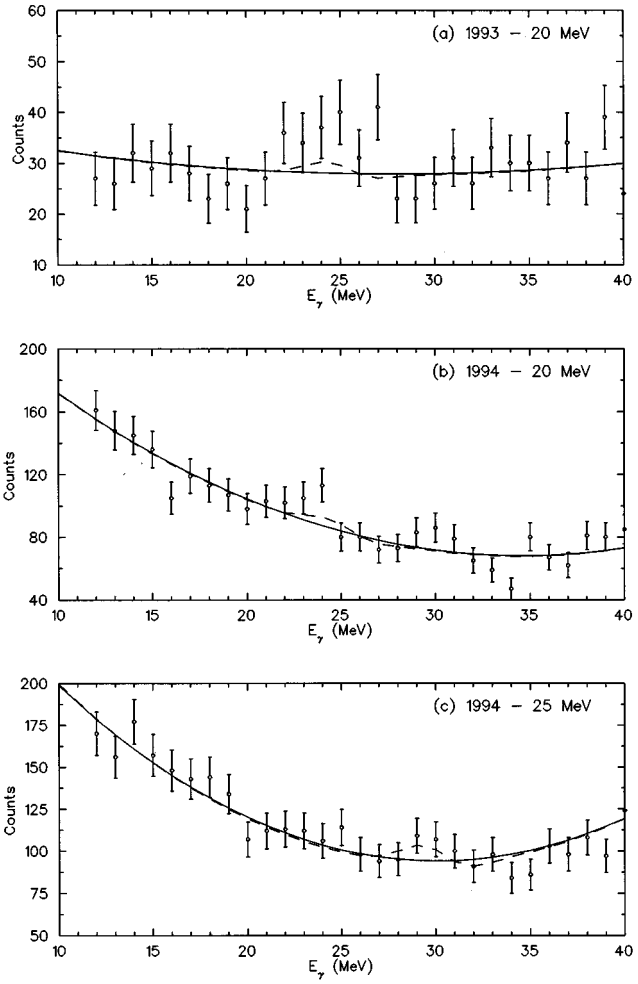

FIG. 10. ^{208}Pb$(\pi^-,\gamma)X$ energy spectra (including background) over the gamma ray energy range of 12–40 MeV. (a) T_π = 20 MeV (1993). (b) T_π = 20 MeV (1994). (c) T_π = 25 MeV (1994). The solid line is a quadratic fit to the continuum, while the dashed line also includes a peak representing the radiative capture transitions to the $1s$ and $2p$ atomic levels with strengths equal to those determined theoretically [15].

where n is the yield per bin, T is the target thickness in atoms/cm^2, $\Delta\Omega$ is the solid angle of the system, ΔE is the gamma ray energy bin width, $N_{\rm inc}$ is the number of incident pions, λ is the instrumental live time, and η is the gamma ray detection efficiency. Typical values of these quantities for each of the three data runs are listed in Table II.

Figure 10, which displays the data (including no-target background) for each of the three runs over the range of gamma ray energies from 12 to 40 MeV, shows the extent to which the statistics were improved for the 1994 runs compared to those of 1993. The size of the continuum background relative to the number of high-energy gamma rays, however, was not significantly improved. Since no gamma ray peaks were clearly discernible in these spectra, several different fits to the spectra (over this energy range) were explored.

The dashed lines in Fig. 10 illustrate the results expected if radiative capture gamma rays to the $1s$ and $2p$ levels occur with a total cross section of 13.5 μb/sr, the value calculated by Nieves and Oset [15]. For the 25 MeV incident

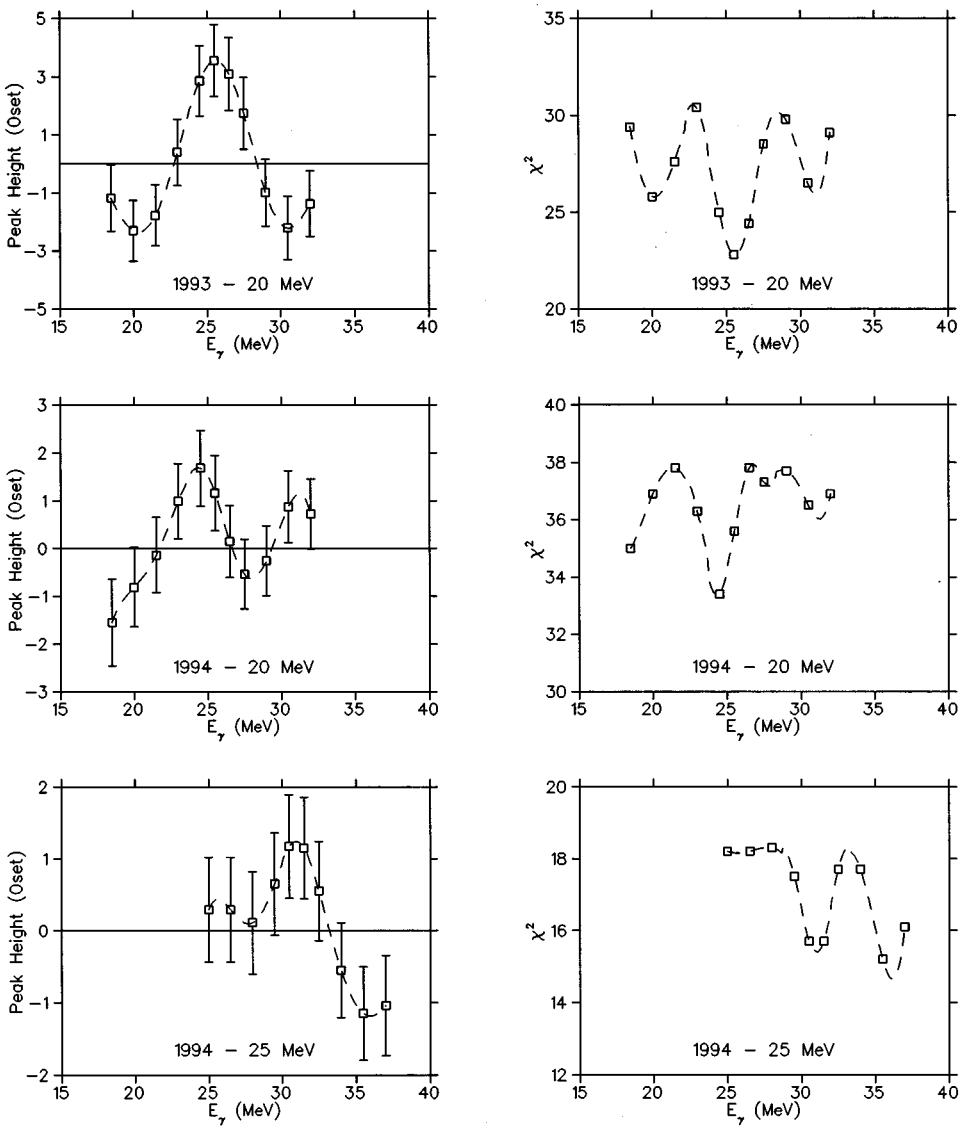

FIG. 11. Dependence of both χ^2 and the height of the fitted peak representing the radiative transition gamma rays to the atomic states, on the energy of these gamma rays. The continuum background is assumed to depend quadratically on energy. The dashed lines are simply intended to guide the eye. For the 25 MeV data, the energy scales (E_γ) are shifted by 5 MeV relative to those for the other cases.

pions, the radiative capture cross sections were taken to be 71% of the 20 MeV values, as suggested by theory [15]. The capture gamma rays were represented as a pair of Gaussian peaks (3 MeV FWHM, our experimental resolution), separated by 1.7 MeV and with an intensity ratio of 2.2:1.0 as indicated by theory [15]. They would thus appear as a single peak in the experimental distributions. In addition to these peaks, it was assumed that the continuum background could be represented as a quadratic function of photon energy. When minimizing the overall χ^2 of the fit, only the three parameters describing the continuum background were varied.

For comparison, the solid curves of Fig. 10 result when the assumed spectrum is *only* the quadratic background *without* the additional Gaussian peaks included. The resulting combined χ^2 result for all three runs is 86.8 for 84 degrees of freedom, or $1.03/N_{\mathrm{DF}}$. At a confidence level of 0.40, this is consistent with the lack of observation of any gamma ray transitions to the atomic states of interest. However, when the gamma radiative transitions *were* assumed to be present, with cross sections given by theory (shown by the set of three dashed lines), the resulting values of χ^2 decreased by 2–4 units in *each* of the three cases (the number of degrees of freedom was the same as for the preceding ''background-only'' fits).

In order to test whether the improvement was simply a chance result due to the particular choice of gamma ray energies assigned to the peaks, fits to the data were carried out for the quadratic background plus the pair of peaks (separated by 1.7 MeV) but now with the peaks placed at a variety of energies spanning the range from 20 to 35 MeV. This time, the overall intensity of the Gaussian peaks was allowed to vary as well. With an effective pion beam energy midway through the Pb target of 0.5 MeV below the nominal incident beam energy, this range of capture gamma ray energies corresponds to $1s$ (atomic state) binding energies (EB1's) varying between 0 and 15 MeV for the 20 MeV incident pions (and -5–10 MeV for the 25 MeV pions). Although the overall strength of the pair of Gaussians was free and fitted to the data, the relative strength of the $2p$ transition to the $1s$ was fixed at 2.2, as predicted by theory [15].

The results of these fits are shown in Fig. 11. Both the strength of the transitions (relative to that expected by theory [15]) and the value of χ^2 (for 27 degrees of freedom in each case) are plotted as a function of capture gamma ray energy. Although *none* of these results separately provide statisti-

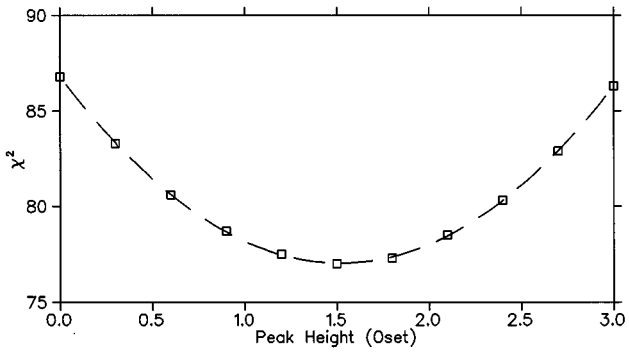

FIG. 12. Summed χ^2 values for all three data runs as a function of radiative capture gamma ray strength relative to theory [15]. The 1*s* binding energy is taken to be 6.0 MeV.

cally significant evidence for the existence of the gamma ray transitions to the atomic states, the fact that *each* set of data is characterized by a χ^2 minimum at an energy close to that expected from theory cannot be ignored. Further, the strengths of the fitted lines are maximized at these energies as well. In addition, the 25 MeV pion run (1994) displays these features at a gamma ray energy which is 5 MeV higher than that of the 20 MeV runs, again consistent with expectation assuming that the capture gamma rays exist. Although the ''strengths'' characterizing these fits vary from one run set to another, they are all in agreement within statistical error. Since the gamma ray energies at which the extrema in these energy dependences occur are generally consistent with those expected from theory [15], they were used to extract the ''experimental'' values of the 1*s* binding energies (EB1's) listed in Table II.

Finally, an experimental estimate of the *strength* of the peaks was obtained by varying the strength of the Gaussian peaks in each of the three data runs, for a pion EB1 value of 6.0 MeV (the average of the three values listed in Table II). For a range of values of the strengths of the Gaussian peaks (from 0 to 3 times that expected theoretically), best fits to each run set were obtained by varying only the three background parameters. The pairs of Gaussian peaks were always constrained to have the same *relative* strengths (2.2) and separation (1.7 MeV) as predicted by theory [15]. By comparing the results to theory (again taking the theoretical value of the capture cross section for 25 MeV pions to be 71% of that for 20 MeV [15]), the results for all three data runs could be combined. Figure 12 displays the resulting *total* value of χ^2 (the sum of the values for each of the three data sets) as a function of the peak height. With 31 data points in each data set, the number of degrees of freedom for this summed plot is 84. Although the value of χ^2 for *zero* peak height is 86.8 as noted earlier (represented by the solid lines in Fig. 10), the overall χ^2 *decreases* for larger values of peak strength, reaching a minimum at a value for the strength of the Gaussian peaks which is 3/2 that predicted by theory [15]. The confidence level appropriate to this minimum ($\chi^2 = 78$) is 67%. This minimum yields a ''best'' fit strength for the combined 1*s* and 2*p* gamma transitions of 20 ± 7 μb/sr, where the error is defined in terms of a $\Delta\chi^2$ of unity. However, with the addition (in quadrature) of systematic errors, assumed to be comparable in magnitude to the statistical, a final value of 20 ± 10 μb/sr results.

VII. CONCLUSIONS

This is the first report of a radiative pion capture experiment attaining the sensitivity required to measure cross sections for radiative capture of negative pions into the ''narrow'' deeply bound atomic states in high-*Z* nuclei whose existence has been predicted by theorists [1,2]. In spite of the fact that our experimental sensitivity was capable of measuring cross sections at the level predicted theoretically, the combination of the presence of a background continuum together with the limited energy resolution of the gamma detector precluded definitive detection of such transitions. Although the results of this experiment are not inconsistent with the lack of any such transition (to a 40% C.L.), the data do imply (at a 67% C.L.) the presence of gamma ray transitions to the tightly bound pionic-atom states in $^{208}\mathrm{Pb}*\pi^-$, with a binding energy of about 6 MeV and a cross section of 20 ± 10 μb/sr at 90° for 20 MeV incident pions. Both values are close to those predicted by theory, 6.7 MeV and 13.5 μb/sr, respectively [15].

VIII. DISCUSSION

The primary goal of this experiment was to exploit the large gamma ray efficiency of a NaI counter, together with the low neutron sensitivity of a segmented version of such a counter to detect the radiative capture gamma rays characterizing the transition of negative pions from the continuum to the narrow low-level atomic states predicted to occur in high-*Z* nuclei [1,2]. Although the segmented NaI counter employed was indeed effective in both suppressing the large neutron-induced background, and providing the necessarily small low-energy tail which was needed for detecting the lower-energy gamma rays at the requisite level, its energy resolution was inadequate to provide an unambiguous identification of the narrow photon lines of interest.

An improvement on the technique described in this paper would require use of high-efficiency photon detectors with energy resolutions of < 1 MeV such as that described in [25], together with the good neutron rejection capability and small low-energy tails characteristic of our system.

Now that clean observation of π-atomic formation has been observed by others in reactions of the type $^{208}\mathrm{Pb}(d,{}^3\mathrm{He})^{207}\mathrm{Pb}*\pi^-$ [14], the emphasis of future experiments will undoubtedly be directed towards obtaining quantitative improvements in our knowledge of the π-nucleus potential. Radiative capture techniques involving real pions in the initial state, as described in this paper, would also provide an important tool for such studies providing that the gamma ray energy resolution can be improved to ~ 0.5 MeV.

ACKNOWLEDGMENTS

The support of the Natural Science and Engineering Research Council of Canada throughout this experiment is gratefully acknowledged. In addition, one of us (K.S.S.) was supported in part by the Yonam Foundation and the Ministry of Education, Korea.

[1] E. Friedman and G. Soff, J. Phys. G **11**, L37 (1985).
[2] H. Toki and T. Yamazaki, Phys. Lett. B **213**, 129 (1988); H. Toki *et al.*, Nucl. Phys. **A501**, 653 (1989).
[3] M. Ericson and T. E. O. Ericson, Ann. Phys. (N.Y.) **36**, 323 (1966).
[4] J. Konijn *et al.*, Nucl. Phys. **A519**, 773 (1990).
[5] A. Olin *et al.*, Nucl. Phys. **A439**, 589 (1985).
[6] C. Tzara, Nucl. Phys. **B18**, 246 (1970).
[7] G. T. Emery, Phys. Lett. **60B**, 351 (1976).
[8] H. Toki, S. Hirenzaki, T. Yamazaki, and R. S. Hayano, Nucl. Phys. **A509**, 653 (1990).
[9] S. Hirenzaki, H. Toki, and T. Yamazaki, Phys. Rev. C **44**, 2472 (1991).
[10] H. Toki, S. Hirenzaki, and T. Yamazaki, Nucl. Phys. **A530**, 679 (1991).
[11] A. Trudel and T. Yamazaki, TRIUMF Annual Report of Scientific Activities, 1991 (unpublished), p. 70.
[12] M. Iwasaki *et al.*, Phys. Rev. C **43**, 1099 (1991).
[13] N. Matsuoka *et al.*, Phys. Lett. B **359**, 39 (1995).
[14] T. Yamazaki *et al.*, in PANIC 96, XIV International Conference on Particles and Nuclei, Williamsburg, Virginia, 1996 (unpublished); T. Yamazaki *et al.*, Z. Phys. A **355**, 219 (1996).
[15] J. Nieves and E. Oset, Phys. Lett. B **282**, 24 (1992); and (private communication).
[16] O. Morimatsu and K. Yazaki, Prog. Part. Nucl. Phys. **33**, 679 (1994).
[17] C. J. Oram *et al.*, Nucl. Instrum. Methods **179**, 95 (1981).
[18] R. Sobie *et al.*, Nucl. Instrum. Methods Phys. Res. A **219**, 501 (1984).
[19] C.J. Virtue, Ph.D. thesis, University of British Columbia, 1987; C. J. Virtue *et al.*, Nucl. Phys. **A517**, 509 (1990).
[20] C. Waltham *et al.*, Nucl. Instrum. Methods Phys. Res. A **256**, 91 (1987).
[21] W. R. Nelson, H. Hirayama, and D. W. O. Rogers, SLAC Report No. 265, Stanford Linear Accelerator Center, 1985 (unpublished).
[22] D. Horvath *et al.*, Phys. Rev. A **41**, 5834 (1990).
[23] K. Nakai *et al.*, Phys. Rev. Lett. **44**, 1446 (1980).
[24] H. W. Baer, K. M. Crowe, and P. Truöl, Adv. Nucl. Phys. **9**, 177 (1977).
[25] A. Hakonsson *et al.*, Nucl. Instrum. Methods Phys. Res. A **273**, 211 (1988).